Thermal conductivity of amorphous thin-film Al-P-O on silicon

River A. Wiedle, Mark Warner, Janet Tate
Department of Physics, Oregon State University, Corvallis, OR 97331, USA
Paul N. Plassmeyer, Catherine J. Page
Department of Chemistry, University of Oregon, Eugene, OR 97403, USA

Abstract

The thermal conductivity, measured by the 3ω method, of amorphous films of $Al_2P_{1.2}O_6$ (AlPO) deposited on Si substrates by an all-aqueous spin-coating technique is 0.93(3) $Wm^{-1}K^{-1}$. The thermal conductivity of a degenerately doped *n*-Si substrate is 85(5) $Wm^{-1}K^{-1}$ and of a more lightly doped *p*-Si substrate is 139(7) $Wm^{-1}K^{-1}$. The AlPO thermal conductivity is independent of film thickness in the range 45 – 200 nm. The total thermal resistance is dominated by the film contribution for film thicknesses above 50 nm, and for smaller thicknesses, interface contributions become significant.

Keywords: Thermal conductivity, interface resistance, 3-omega method, amorphous dielectric, thin-film, AlPO, solution processes

1 Introduction

In many technologically relevant materials, the thermal properties are of great importance. In thermoelectric devices, the Seebeck coefficient produces the primary functionality and, along with the thermal and electrical conductivities, establishes the figure of merit. In other devices, the thermal properties of the constituent materials may determine whether the material is a viable candidate for an application, even if the thermal properties do not constitute the primary functionality. For example, an excellent dielectric may not be useful as a gate insulator if the thermal boundary resistance is too high and increases the phonon temperature during switching. Recently, amorphous thin-

film and nanolaminate dielectrics of aluminum phosphate (AlPO) and hafnium and zirconium sulfates (HafSOx and ZircSOx) have been produced by an all-aqueous spin-coating method [1,2,3,4]. These films are amorphous, dense, and pin-hole free even at 2 nm thickness. Amorphous AlPO dielectric films produced in this manner have proven to be high performance gate insulators in transparent transistors [5]. Amorphous HafSOx and ZircSOx films in some cases can be patterned by using ultraviolet light or electron beams during processing, which may enable mask-free patterning on a large scale [6,7]. Such films have already been used to demonstrate 10-nm half pitch patterning, which pushes the scale of lithography well below the present 22-nm standard [8]. Given the potential of such films to be used in electronic devices, their thermal, optical, and mechanical properties must be established along with the unique chemistry that defines them.

Oxide dielectrics on Si substrates are the subject of significant research because high-dielectric alternatives to the SiO_2 native oxide are needed in conventional electronics. Si is also a substrate for thermoelectric devices, so the evaluation of the thermal properties of thin films on Si is important. Panzer *et al*. [9] reported thermal properties of HfO_2. They used time-domain thermoreflectance, and found that the thermal conductivity κ_{HfO2} of 5-nm to 20-nm films on Si depended on the film morphology and thickness and fell in the range 0.49 - 0.95 $Wm^{-1}K^{-1}$ at room temperature. They were further able to measure thermal boundary resistances of the $HfO_2/SiO_2/Si$ stacks at $3 - 12 \times 10^{-9}$ m^2KW^{-1}. Gabriel and Talghader [10] measured thermal conductivity of 50 – 100 nm films of SiO_2, HfO_2 and Al_2O_3 and combinations thereof on silicon substrates by a variation of the 3ω method that we report here.

In this work, we use the 3ω method to determine the thermal conductivity of amorphous thin-film $Al_2P_{1.2}O_6$ films (45-200 nm) on Si substrates. The 3ω method was developed for bulk dielectrics [11] and has been applied to thin-film dielectrics [12]. We describe the AlPO film preparation, and measurements of the film thickness, thermal conductivity and interface resistance with the substrates. We discuss the results, and also report the

thermal conductivity and thermal diffusivity of the Si substrates, and the effect of *n*- and *p*- dopants on those properties.

2 Experiment

2.1 AlPO film preparation

Thin films of amorphous $Al_2P_{1.2}O_6$ (AlPO) are prepared on Si wafers by an all-aqueous, spin-coating method [1]. Starting materials for the AlPO precursor are $Al(OH)_3$ (76.5% min, Alfa Aesar), trace metal grade HNO_3 (70% w/w, Fisher) and H_3PO_4 (85% w/w, EMD Chemicals). $Al(OH)_3$ is added to volumetric flasks with a target concentration of 0.68 M for each parent solution. The $Al(OH)_3$ is then submerged in 18.2 MΩ cm deionized H_2O and two mole equivalents of nitric acid are added drop-wise to the flask while the contents are stirred. The aluminum hydroxide and nitric acid solution is heated and stirred at 85 °C overnight. H_3PO_4 is then added drop-wise to achieve an Al^{3+}:PO_4^{3-} ratio of 1:0.6. This solution is diluted to the desired concentration with 18.2 MΩ cm H_2O and held at 85 °C for an additional 24 h. The solutions are checked by laser scattering for the presence of small, undissolved particles.

Polished *n*-type (As-doped, 0.0010 Ωcm) or *p*-type (B-doped, 50 Ωcm) (100)-oriented silicon substrates from SumCo are sonicated in a bath of 5% Contrad 70, 95% 18.2 MΩ cm H_2O (v/v) at 45°C for 60 min. AlPO precursors are deposited from a syringe through a 0.45-µm polytetrafluoroethylene filter onto the Si substrate. Solution-covered substrates are rotated at 3000 rpm for 30 s. Samples are immediately transferred to a 300 °C hotplate for 30 s. This process is repeated to achieve the desired film thickness, after which the films are annealed in air at either 450 °C or 600 °C for 30 min. In this work, we study two series of 1-, 2-, 3-, and 4-layer AlPO films on *p*-type Si. One series is annealed at 450 °C and the other at 600 °C. We also study one series on *n*-type Si annealed at 600 ˚C.

2.2 Film Characterization

X-ray reflectivity (XRR) measurements are made on a Bruker D8 Discover X-ray spectrometer using 1.5418 Å Cu-Kα radiation to determine the film density and thickness of each single-layer film. These data are analyzed using the EVA software package for peak finding, and a modified form of the Bragg Equation using Snell's Law as a correction to the angle between incident ray and the scattering planes. The XRR patterns are also modeled using Bede Refs modeling software. The films are modeled as an AlPO layer on a thin (1.2 nm) layer of SiO_2 on a substrate of silicon with infinite thickness. The models are restricted to fitting the thickness and density of each layer and the roughness of each interface. Ellipsometry measurements (J.A. Woollam Co., Inc. M2000X-210) are carried out on all films over the range 1.240-5.168 eV and at angles of 55˚, 60˚, and 65˚. Data are fit to a Cauchy model assuming a 1-nm native SiO_2 interface between the film and an infinitely thick Si substrate.

2.3 Thermal conductivity

The 3ω method is used to measure thermal conductivity and interface resistance [11,12]. A thin metal film deposited on a thick substrate and supplied with an oscillating current acts simultaneously as an oscillating heat source and as a resistance temperature detector to measure the effect of this heating (Fig. 1). The current I at frequency $\omega = 2\pi f$ increases the temperature of the heater/substrate stack in proportion to the input power, $P=I^2R$, and therefore produces a small modulation of the temperature at frequency 2ω. The resistance R of the heater increases linearly with the temperature, so R is also modulated at 2ω, and the voltage across the resistor, $V = IR$, therefore contains a small third harmonic component, $V_{3\omega}$, which is measured with an SR 850 lock-in amplifier. The circuit is shown in Fig. 2. The heater response in the inset to Fig. 2 clearly shows the third harmonic. The in-phase and out-of-phase components of $V_{3\omega}$ depend on the thermal conductivity κ and diffusivity D of the substrate, the geometry of the heater, the input power, and the thermal coefficient of resistance (TCR) α of the heater. $V_{3\omega}$ is related by readily-measured experimental parameters to an equivalent temperature increase ΔT or to an equivalent thermal resistance, R_{th}:

$$R_{th} = \frac{2bl}{P}\Delta T = \frac{4blV_{3\omega}}{P\alpha V_{1\omega}} \qquad [1]$$

where $V_{1\omega}$ is the applied voltage at frequency ω, and 2*b* and *l* are the width and length of the heater, respectively. The frequency of excitation *f* is varied over a range that keeps the thermal penetration depth small compared to the substrate thickness, but large compared to the heater width, and the data are fitted to the model of Cahill [11] to extract the material parameters κ and *D*:

$$\Delta T = \frac{P}{\pi l \kappa} \int_0^\infty \frac{\sin^2(kb)}{(kb)^2 \sqrt{k^2 + i2\omega / D}} dk \qquad [2]$$

To measure the thermal conductivity of a dielectric thin film using this technique, the thin film of thickness *d* and thermal conductivity κ_f is inserted between the heater and the bulk substrate, whose thermal properties are well known. The film adds an additional thermal resistance, determined by κ_f and *d* [12]:

$$\Delta R_{th} = \frac{d}{\kappa_f} \qquad [3]$$

The thermal resistance of otherwise identical films of different thicknesses is measured, and a plot of ΔR_{th} *vs*. *d* should yield a linear relationship provided that the film is thin enough ($d << 2b$) that heat flow from the heater through the film to the substrate is uniform (negligible edge effects). The inverse slope of the plot gives the thermal conductivity of the film material and the intercept gives the sum of the thermal resistances of the film/substrate and heater/film interfaces.

In this work, four 180-nm thick Al heaters with length *l* =1 mm and widths 2*b* = 10 μm, 15 μm, and 20 μm are thermally deposited through a photolithographically-produced mask onto each AlPO/Si stack (Fig. 1). The stack is heated to 150 ˚C to ensure good heater adhesion and thereby minimize thermal interface resistance. The TCR near room temperature is precisely determined for individual heaters using a microthermocouple to monitor the temperature at the heater as the stack is heated on a hot plate, and a low-frequency current-voltage curve to determine the resistance at each temperature. Typical heater resistances are 15-30 Ω, and TCRs are 0.0030 – 0.0038 K^{-1}. With film thicknesses of 50-200 nm, *d*/2*b* is 5-20 x 10^{-3}, so the condition for sensible interpretation

of the thin-film measurements of the thermal resistance is well satisfied. The input power is 25-50 Wm^{-1} RMS resulting from a 400-1000 mV RMS voltage applied across the heater. The temperature rise of the heater is less than 1 K over the measured frequency range.

3 Results

Fig. 3 is an XRR spectrum of a single coat of AlPO on an *n*-Si substrate. In this example, the fit to the modulation in reflectivity yields a thickness of 48.2 nm (46.1 nm) for a film annealed at 450 ˚C (600 ˚C), a surface roughness of 0.56 nm (0.49 nm) and a density of 2.35 g cm^{-3} (2.36 g cm^{-3}). For comparison, the density of single crystal $AlPO_4$ is 2.57 g cm^{-3}. Ellipsometry confirms the XRR thickness measurements and shows that multi-layer films are close to integer multiples of the single layer thickness. The thicknesses used were taken from ellipsometery measurents and have a typical error of 0.5%.

In the main panel of Fig. 4, the thermal conductivity measurement of a Corning 1737 glass substrate are presented as thermal resistance (Eq. 1) as a function of frequency to demonstrate the validity of the 3ω method. Both in-phase and out-of-phase components are shown for a wide frequency range, and the data accurately fit the model of Cahill [11] over the entire range with two free parameters $\kappa_{1737} = 0.90$ $Wm^{-1}K^{-1}$, and $D_{1737} = 0.7$ mm^2 s^{-1}, which should be compared with published values $\kappa_{1737} = 0.91$ $Wm^{-1}K^{-1}$, and $D_{1737} = 0.50$ mm^2 s^{-1} [13]. Our larger D value derives from the fact that Eq. 2 attributes all thermal resistance to the bulk substrate and neglects thermal interface resistance. The fit parameter D absorbs the poorly-known thermal interface resistance and therefore increases. However, because the interface resistance causes a *constant* shift of R_{th} at low frequencies, it has a negligible effect on the determination of κ, which is derived predominantly from the *slope* of R_{th} vs log f [11,12]. The excellent agreement of κ values is therefore expected. The inset to Fig 4 shows the in-phase component for one AlPO/*n*-Si and one AlPO/*p*-Si stack in the frequency range where R_{th} *vs*. log f is linear. The thermal conductivity of the Si substrate is the fitting parameter that determines the slope,

and we find $\kappa_{n\text{-Si}} = 85(5)$ $Wm^{-1}K^{-1}$ and $\kappa_{p\text{-Si}} = 139(7)$ $Wm^{-1}K^{-1}$. The uncertainly reflects values obtained for the same substrate using different AlPO films.

Fig. 5(a) is a plot of the thermal resistance of four AlPO/*p*-Si stacks as a function of frequency. The AlPO films are identically prepared, varying only in the number of depositions and hence the final thickness, which ranges from 50 – 200 nm. In this thickness range, the thermal resistivity *vs.* log frequency is linear with the slope determined by the conductivity of the Si substrate, κ_{Si}. The slopes are identical (within about 5%), and the best-fit κ_{p-Si} is used to calculate the thermal resistance of the bare Si substrate from Eq. 3 using a value for the diffusivity of $D = 88$ mm^2s^{-1}. The calculated Si substrate thermal resistance is displayed as a solid line in Fig. 5(a).

The difference ΔR_{th} between the measured AlPO/*p*-Si thermal resistance and the calculated Si thermal resistance is constant over the frequency range for each film. ΔR_{th} gives the thermal resistance of the AlPO film plus any thermal resistance associated with interfaces, *e.g*. heater/AlPO, AlPO/Si, and the thermal resistance of the Si native oxide must also be included in this interface resistance. ΔR_{th}, is plotted as a function of the thickness of the film in Fig. 5(b). Thermal interface resistances are not known *a priori*, but careful attention to film and heater preparation conditions allows us to assume that the interface resistances are similar in all AlPO/Si stacks in a series. This assumption is supported by the observed *linear* increase in ΔR_{th} with AlPO thickness. The inverse slope of the ΔR_{th} *vs*. *d* plots gives the thermal conductivity of the thin-film AlPO. In the case of the film series represented in Fig. 5(b), $\kappa_{AlPO} = 0.94(3)$ $Wm^{-1}K^{-1}$. We have made similar measurements on the same AlPO film series using heaters with a different geometry, and with a second set of measurements several months later. We measured a different series of AlPO films annealed at 450 ˚C on *p*-Si, and another series annealed at 600 ˚C on n-Si. We measure a range of values 0.91 - 0.97 $Wm^{-1}K^{-1}$ as listed in Table 1. We see no statistically significant difference between the thermal conductivities of films annealed at 450 ˚C and 600 ˚C. The uncertainties for individual measurements listed in Table 1 derived from the quadrature combination of uncertainties in the heater length and width, the thermal coefficient of resistance of the heater, and the 1ω current and voltage

in the circuit, as well as the uncertainty in the slope in Fig. 5. The weighted average of the individual thermal conductivities is 0.93(3), with the uncertainty being the standard deviation of the mean.

The zero-thickness intercept, 3.4×10^{-8} m^2KW^{-1}, in Fig. 5(b) determines, in principle, the interface resistance in the system. However, any error in the calculation of the Si substrate thermal resistance would be absorbed in this value. The primary error in the Si thermal resistance calculation comes from incomplete knowledge of the diffusivity, *D*, which cannot be determined from the data in this limited frequency range. Variation of *D* by 50% from the single crystal value of 88 mm^2s^{-1} produces change of less than 10% in the calculated thermal resistance of Si, which is negligible on the scale of Fig. 5. We therefore conclude that the total interface resistance in our system is 3.4×10^{-8} m^2KW^{-1}, which translates to an interface thermal conductance of 0.03 GW m^{-2} K^{-1}.

4 Discussion

The room temperature thermal conductivity of AlPO amorphous films, 0.93(3) $Wm^{-1}K^{-1}$, at the lower end of the range of typical fused SiO_2 thermal conductivities, which vary considerably depending on the glass additives. It is very similar to that of Corning 1737, a boro-aluminosilcate glass (0.907 $Wm^{-1}K^{-1}$) [13], and lower than Corning 7913 (κ_{7913} = 1.38 $Wm^{-1}K^{-1}$) [14] and Corning Eagle XG (4.56 $Wm^{-1}K^{-1}$) [15]. The most useful comparison to the present work is the thermal conductivity of thin-film oxides on Si. Panzer *et al.* [9] report κ_{HfO2} = 0.49 - 0.95 $Wm^{-1}K^{-1}$ depending on thickness for HfO_2 films of thickness 6 – 20 nm. Gabriel and Talghader [10] measure the thermal conductivity of 50-100 nm SiO_2 thermal oxide as κ_{SiO2} = 1.5 -1.6 $Wm^{-1}K^{-1}$, of 100-nm HfO_2 on Si as κ_{HfO2} = 1.72 $Wm^{-1}K^{-1}$, and alumina as κ_{Al2O3} = 2.59 $Wm^{-1}K^{-1}$. They also report the thermal conductivity of several hafnia-alumina nanolaminates at 1.07 $Wm^{-1}K^{-1}$. Amorphous AlPO on Si is therefore one of the lower-thermal-conductivity glasses.

The thermal boundary resistances of the $HfO_2/SiO_2/Si$ stacks measured by laser excitation of the heat pulse were in the range of $3 - 12 \times 10^{-9}$ Km^2W^{-1} [9]. In the present work, the $AlPO/SiO_2/Si$ stacks exhibit an interface resistance of 3.4×10^{-8} m^2KW^{-1}, about an order of magnitude higher. Our measurement required an additional thermal interface (heater/AlPO). Phonon-limited thermal conduction across typical solid/solid interfaces is typically 1 $GWm^{-2}K^{-1}$ [16], so we presume that the heater/AlPO interface gives the dominant contribution, and that interface must be investigated before we can make a judgment about the AlPO/Si interface.

The thermal conductivity value of $\kappa_{p\text{-Si}}$ = 132-146 $Wm^{-1}K^{-1}$ for the 50 Ωcm *p*-Si substrate is significantly higher than $\kappa_{n\text{-Si}}$ = 80-90 $Wm^{-1}K^{-1}$ for the 0.0010 Ωcm *n*-Si substrate, indicating that the electrical charge carriers in Si provide a significant source of phonon scattering that reduces the thermal conductivity. These electrical resistivities translate to carrier concentrations of about $p = 3 \times 10^{14}$ cm^{-3} and $n = 6 \times 10^{19}$ cm^{-3} respectively [17]. Our values of the room-temperature Si thermal conductivities at these carrier concentrations are in reasonable agreement with those reported by Rowe and Bhandari [18] of 155 $Wm^{-1}K^{-1}$ for *p*-type Si ($p = 4.2 \times 10^{14}$ cm^{-3}) and 90 $Wm^{-1}K^{-1}$ for *n*-type Si (interpolated from values for $n = 2\times10^{19}$ cm^{-3} and 17×10^{19} cm^{-3}).

5 Conclusions

The room-temperature thermal conductivity of amorphous AlPO thin films on Si produced by an all-aqueous spin-coating technique is 0.93(3) $Wm^{-1}K^{-1}$ as measured by the 3ω technique on several different samples. This low thermal conductivity suggests application as a thermal barrier. More generally, we have shown that the 3ω technique is a simple and reliable way to simultaneously measure the thermal conductivity of a thin film and its substrate, but the need for a metallic heater introduces another thermal interface that must be well characterized before conclusions about other thermal interfaces in the system can be drawn. Our results also indicate that electrical carriers in Si provide a phonon-scattering mechanism that significantly decreases its thermal conductivity.

Acknowledgements

We thank Matthew Oostman for initial development of the data acquisition software, and the Douglas Keszler laboratory for contributing samples for preliminary measurements. We thank REU students Rose Baunach and James Cutz for their measurements on one series of films presented in Table 1. This work was conducted in part in the Center for Sustainable Research Chemistry supported by the National Science Foundation under CHE-1102637, using the Materials Synthesis and Characterization Facility (MASC) at Oregon State University.

References

[1] S. T. Meyers, J. T. Anderson, D. Hong, C. M. Hung, J. F. Wager, D. A. Keszler, Chem. Mater. 19 (2007) 4023.

[2] J. T. Anderson, C. L. Munsee, C. M. Hung, T. M. Phung, G. S. Herman, D. C. Johnson, J. F. Wager, D. A. Keszler, Adv. Funct. Mater. 17 (2007) 2117.

[3] K. Jiang, S. T. Meyers, M. D. Anderson, D. C. Johnson, D. A. Keszler, Chem. Mater. 25 (2013) 210**.**

[4] M. Alemayehu, J. E. Davis, M. Jackson, B. Lessig, L. Smith, J. D. Sumega, C. Knutson, M. Beekman, D. C. Johnson, D. A. Keszler, Solid State Sci. 13 (2011) 2037.

[5] K. M. Kim, C. W. Kim, J-S. Heo, H. Na, J. E. Lee, C. B. Park, J-U. Bae, C.-D. Kim, M. Jun, Y. K. Hwang, S. T. Meyers, A. Grenville, D. A. Keszler, Appl. Phys. Lett. 99 (2011) 242109.

[6] J. Stowers, D. A. Keszler, Microelectronic Engineering 86 (2009) 730.

[7] A. Telecky, P. Xie, J. Stowers, A. Grenville, B. Smith, D. A. Keszler, J. Vac. Sci. Technol. B 28 (2010) C6S19.

[8] Y. Ekinci, M. Vockenhuber, B. Terhalle, M. Hojeij, L. Wang, T. R. Younkin, SPIE Proceedings Vol. 8322 (2012), Extreme Ultraviolet (EUV) Lithography III, P. P. Naulleau, O. Wood II (eds) 83220W (DOI: 10.1117/12.916541).

[9] M. A. Panzer, M. Shandalov, J. A. Rowlette, Y. Oshima, Y. W. Chen, P. C. McIntyre, K. E. Goodson, IEEE Electron Device Letters 30 (2009) 1269.

[10] N. T. Gabriel, J. J. Talghader, J. Appl. Phys. 110 (2011) 043526.

[11] D. G. Cahill, Rev. Sci. Instr. 61, 802-808 (1990); *Erratum* Rev. Sci. Instr. 73 (2002) 3701.

[12] J. H. Kim, A. Feldman, D. Novotny, J. Appl. Phys. 86 (1999) 3959.

[13] Corning MIE 101, p. 1, Corning Incorporated (2003) http://www.vinkarola.com/pdf/Corning Glass 1737 Properties.pdf accessed 12 February 2013.

[14] Corning data sheet, Corning Incorporated (2001) http://www.coresix.com/images/Vycor_7913.pdf accessed 19 March 2013.

[15] Corning MIE 302, p. 2, Corning Incorporated (2010) http://www.corning.com/WorkArea/showcontent.aspx?id=48971 accessed 19 March 2013.

[16] D. G. Cahill, W. K. Ford, K. E. Goodson, G. D. Mahan, A. Majumdar, J. Appl. Phys. 93 (2003) 793.

[17] Semiconductor Devices: Physics and Technology, S.M. Sze, Wiley (1985) p. 38.

[18] D. M. Rowe and C. M. Bhandari, Prog. Cryst. Growth Charact. Mater. 13 (1986) 233.

Table Caption:

Table I: Results of thermal conductivity measurements of several series of AlPO films.

Figure Captions:

Fig. 1. Thin-film thermal conductivity measurement configuration. A metal heater/sensor is deposited on a thin film and substrate. There is thermal interface resistance at the film/heater and the film/substrate boundary.

Fig. 2. 3ω measurement circuit. The subtraction circuit uses TI INA128P instrumentation amplifiers. (Inset) Oscilloscope trace of the voltage across the metal heater. The upper trace is the total voltage and the lower trace has the 1ω component reduced to emphasize the small 3ω component.

Fig. 3. X-ray reflectivity (main panel) measurement of a single coating of AlPO on Si and ellipsometry (inset) measurements on multilayered (1-4 layers) AlPO on Si films. The angle of incidence is 65˚.

Fig. 4. R_{th} *vs*. log *f* for Corning 1737 glass and (inset) *n*- and *p*-Si. In the main panel, the dark line is the experimental data and the light line is the model due to Cahill [11].

Fig. 5. (a) R_{th} *vs*. log *f* for a series of AlPO films of different thicknesses on a *p*-Si substrate. (b) Change in R_{th} *vs.* film thickness for the AlPO film series.

Table I

Series	Description	$2b$ (μm)	#points	κ_{AlPO}
1	AlPO/*p*-Si (600 C)	15	4	0.94(7)
1	AlPO/*p*-Si (600 C)	20	3	0.95(5)
1*	AlPO/*p*-Si (600 C)	15	4	0.93(7)
2	AlPO/*p*-Si (450 C)	20	4	0.92(5)
3	AlPO/*n*-Si (600 C)	20	4	0.97(7)
Weighted average				0.93(3)

Table I: results of thermal conductivity measurements of several series of AlPO films.

*Measured 6 months later

Figure 1

Click here to download high resolution image

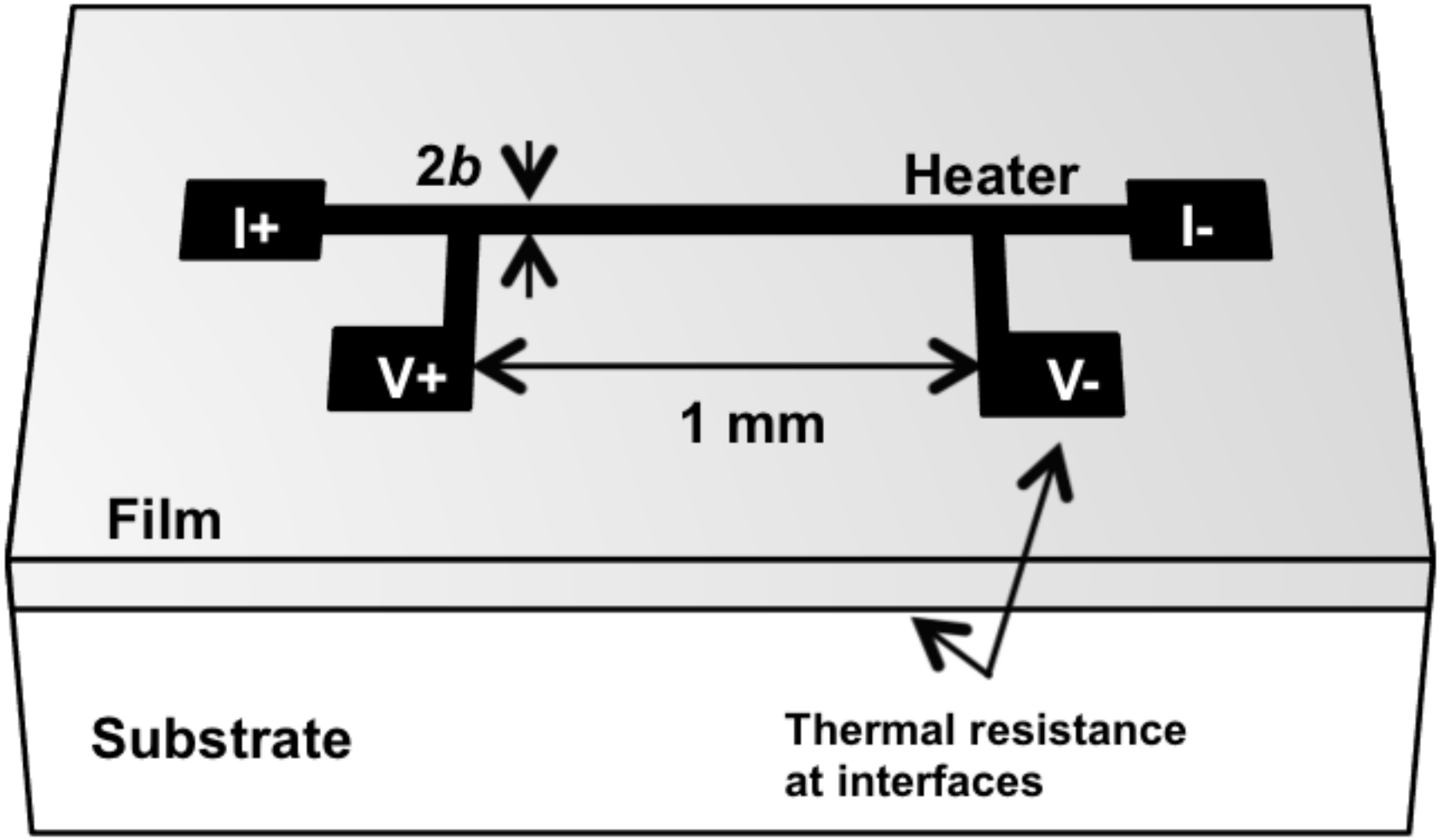

Figure 2

Click here to download Figures (if any): circuit.pptx

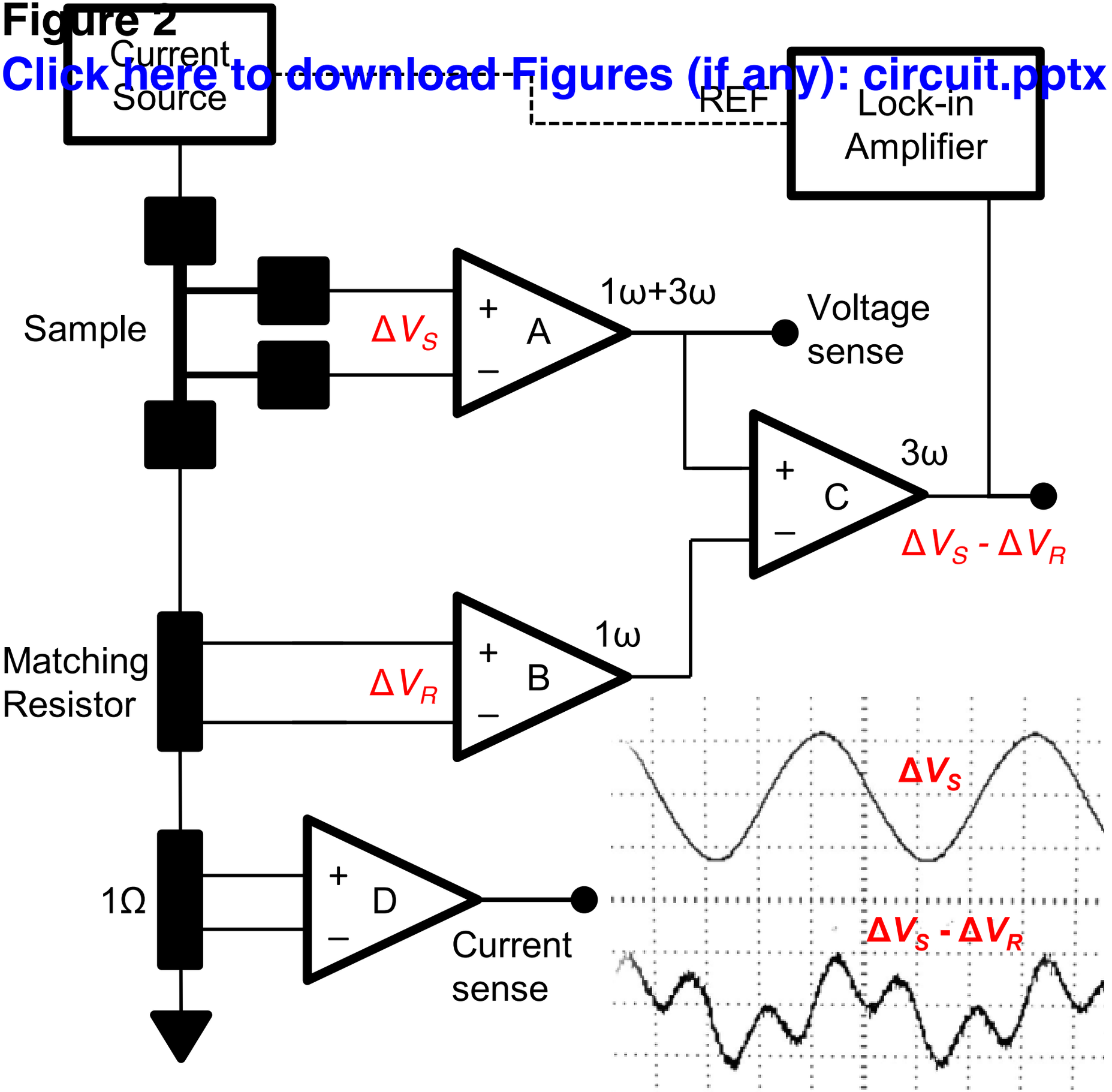

Figure 3

Click here to download high resolution image

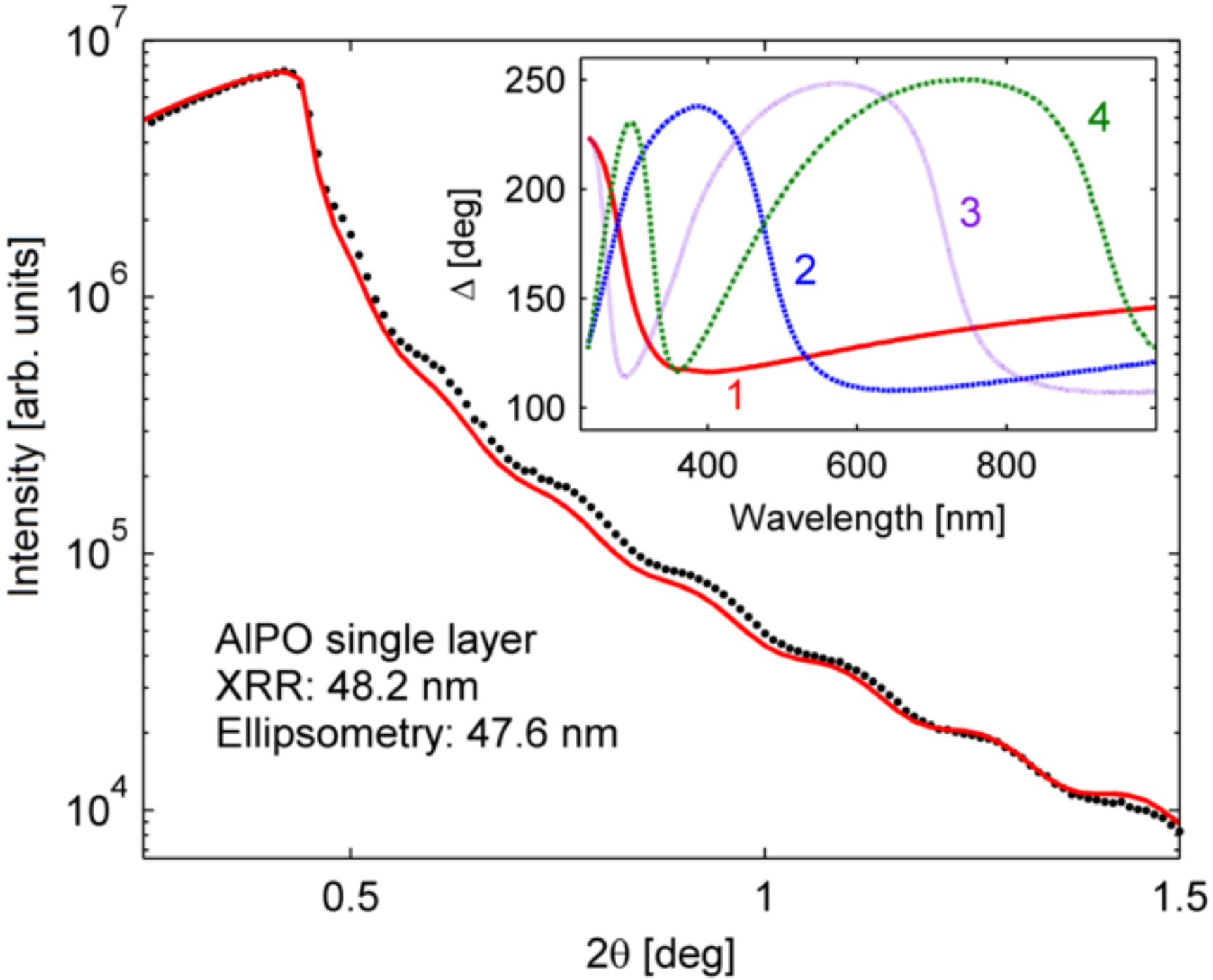

Figure 4
Click here to download high resolution image

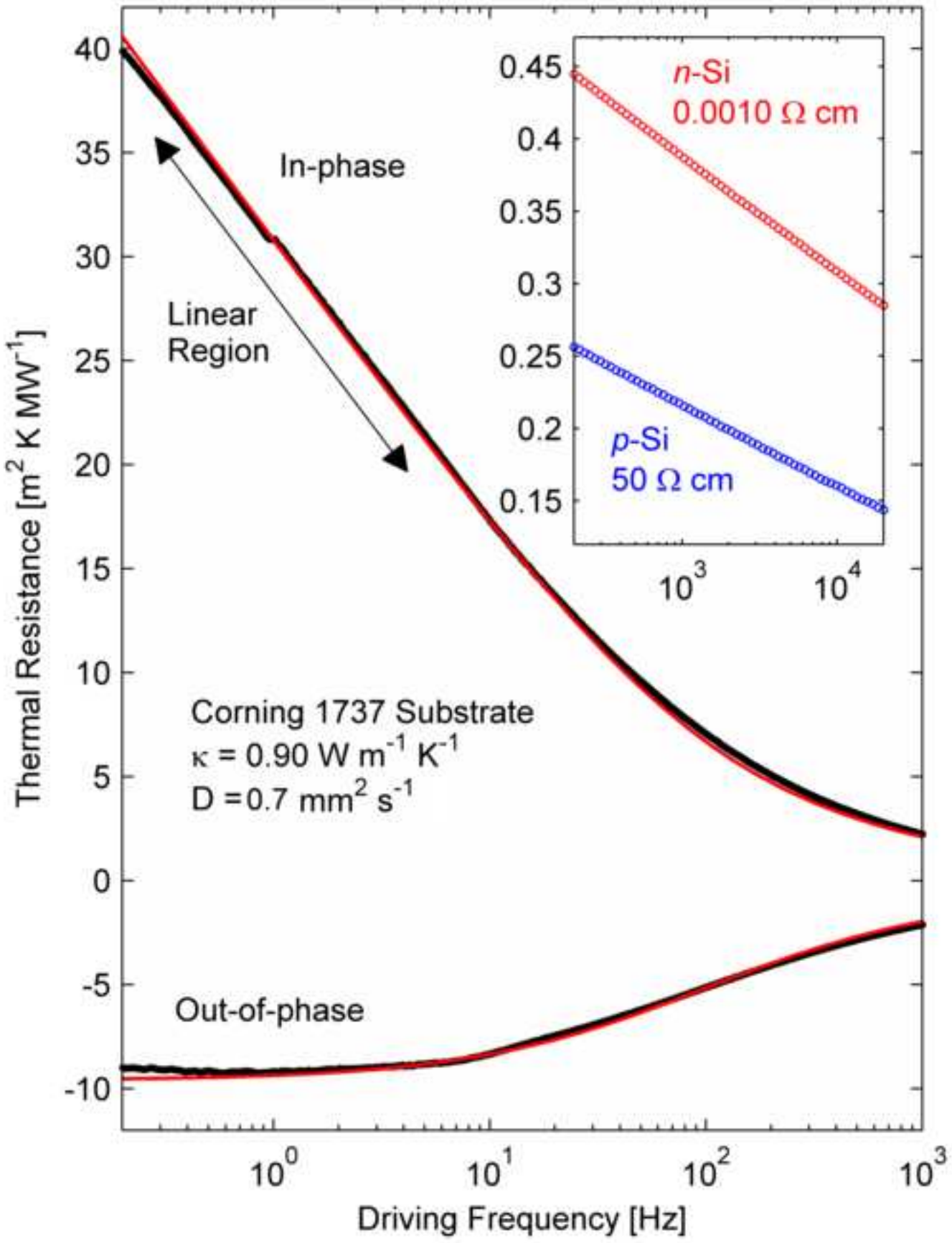

Figure 5a
Click here to download high resolution image

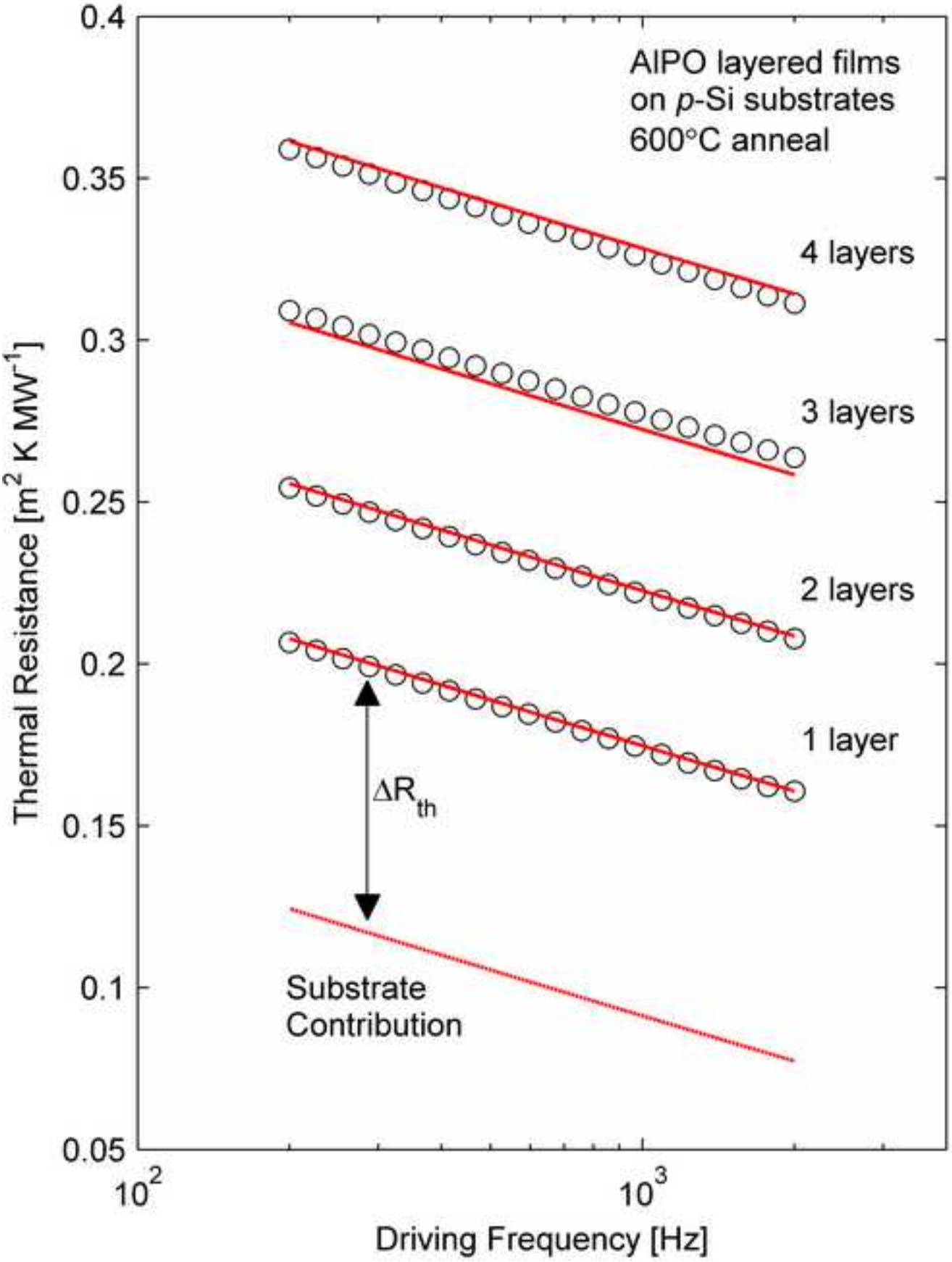

Figure 5b
Click here to download high resolution image